Journal of Colloid and Interface Science 365 (2012) 90–96

Contents lists available at SciVerse ScienceDirect

Journal of Colloid and Interface Science

www.elsevier.com/locate/jcis

Ultrathin and nanostructured ZnO-based films for fluorescence biosensing applications

Cristina Satriano [a,*], Maria Elena Fragalà [a], Yana Aleeva [b]

[a] Dipartimento di Scienze Chimiche, Università degli Studi di Catania and INSTM, viale Andrea Doria n. 6, 95125 Catania, Italy
[b] Scuola Superiore – Università degli Studi di Catania, Dipartimento di Scienze Chimiche, viale Andrea Doria n. 6, 95125 Catania, Italy

ARTICLE INFO

Article history:
Received 12 June 2011
Accepted 9 September 2011
Available online 17 September 2011

Keywords:
ZnO thin film
MOCVD–colloidal lithography
Biosensing
Protein adsorption
Fluorescence recovery after photobleaching

ABSTRACT

The fluorescence-based sensing capability of ultrathin ZnO–SiO_2 nanoplatforms, deposited by an integrated approach of colloidal lithography and metal organic chemical vapor deposition, has been investigated upon adsorption of fluorescein-labeled albumin, used as model analyte biomolecule. The protein immobilization process after spontaneous adsorption/desorption significantly enhances the green emission of the different ZnO-based films, as evidenced by scanning confocal microscopy, corresponding to a comparable protein coverage detected by X-ray photoelectron spectroscopy. Moreover, experiments of fluorescence recovery after photobleaching evidence that the protein lateral diffusion at the biointerface is affected by the chemical and/or topographical patterning of hybrid ZnO–SiO_2 surfaces. The used approach is very promising for biomolecular detection applications of these ZnO–SiO_2 nanoplatforms, by simple sizing of the 2D vs. 3D patterning design, which in turn is accomplished by the fine tuning of the integrated colloidal lithography–chemical vapor deposition processes.

1. Introduction

Development of advanced substrates for biomolecular sensing is critically related to multitasking capability, sensitivity and specificity aspects. An emergent field of research for various applications in biomolecular detection is the innovative assembly of zinc oxide nanostructures [1,2]. Indeed, zinc oxide (ZnO) is an extremely versatile material even at the nanoscale, due to processing through many synthetic routes [3], easy integration into periodically patterned nanoplatforms [4–6], desirable optical properties [7] and stability in typical biomolecular detection environments [8]. Moreover, nanostructured ZnO materials possess high surface area and good biocompatibility and biodegradability [9] that make them very advantageous as platforms to detect the immobilization of glucose [10], cholesterol [11], DNA [5,12] and several other biomolecules [13–16]. In particular, examples of the use of nanoscale ZnO in the enhanced fluorescence detection of protein interactions have shown that ZnO can act as an excellent signal-intensifying substrate for a wide range of biomolecules [1,17,18]. Recently, the ultra-sensitivity of zinc oxide nanorod arrays in conjunction with a FITC-labeled affinity peptide has been successfully demonstrated for biosensing applications [19].

As to the fabrication of nanostructured platforms, in recent years, the synthetic strategy of combining colloidal lithography (CL) with several deposition techniques, including metal-organic chemical vapor deposition (MOCVD) [18,21], self-assembled monolayers [22], plasma processes [23,24], drop casting [25] and metal sputter/coating processes [26,27], has been proven effective to fabricate chemical/topographical patterns for driving protein adsorption and cell adhesion.

In previous works, we demonstrated the successful process integration of MOCVD processes, at unusual mild conditions (i.e., low temperature/short deposition time), with colloidal lithography to assemble ZnO ultrathin films into periodic arrays of micro/nanopores [4,20], exhibiting sensitive and specific detection of surface immobilized proteins [18]. To proceed with such investigations, we focus herein on the chemical, topographical and optical characterization of these ultrathin ZnO films and hybrid ZnO–SiO_2 micropore arrays. A multitechnique approach involving X-ray photoelectron spectroscopy (XPS), scanning electron microscopy (SEM) and laser scanning confocal microscopy (LSM) has been used.

Moreover, the hybrid biointerface with fluorescein-labeled albumin, used as model analyte biomolecule, is investigated by means of fluorescence recovery after photobleaching (FRAP) experiments. The results demonstrate that such ultrathin films have great potential as innovative fluorescence-sensing substrates, offering the possibility of sizing the 2D vs. 3D design of the ZnO–SiO_2 array (through the fine tuning of CL and MOCVD conditions), which, in turn, affects the individual addressability of the biomolecular detection.

* Corresponding author. Fax: +39 095 580138.
E-mail address: csatriano@unict.it (C. Satriano).

0021-9797/$ - see front matter © 2011 Elsevier Inc. All rights reserved.
doi:10.1016/j.jcis.2011.09.014

2. Materials and methods

2.1. Metal-organic chemical vapor deposition (MOCVD) and integrated MOCVD–colloidal lithography

ZnO deposition was performed in a horizontal hot-wall MOCVD reactor at a pressure of about 5 Torr, by using $Zn(tta)_2$tmeda precursor, Ar (250 sccm, carrier gas) and O_2 (250 sccm, reaction gas) [28,29]. The substrates used for the deposition were (i) monopolished (100) silicon (University Wafer), for XPS and SEM analyses, and (ii) glass coverslip (Biopthecs), for LSM measurements. Three sets of samples were produced at the following temperature/time deposition conditions, namely 300 °C/40 m, 400 °C/5 min and 400 °C/60 min (thereafter named, respectively, ZnO-1, ZnO-2 and ZnO-3) to end up with 12 different samples.

A parallel set of samples was prepared by integrating the MOCVD (400 °C/5 min) with the CL technique (ZnO-2 NP samples). Briefly, the substrates were masked by a 2D close-packed monolayer of polystyrene colloids of 1 micrometer of diameter (Sigma), self-assembled by dewetting (1 wt.% in aqueous solution), MOCVD was performed, and colloids were removed [4,20].

2.2. Protein immobilization at the ZnO–SiO_2 surfaces

Fluorescein isothiocyanate–labeled albumin (FITC-albumin) was purchased as powder (Sigma) and used as received after dissolving in 0.01 M phosphate buffer saline solution containing 0.003 M KCl and 0.14 M NaCl (PBS, pH 7.4 at 25 °C, Sigma).

As indicated by the supplier, the chromophore is coupled to the protein through the ε-amino group of lysines of the albumin, and the labeling density corresponds to a degree of substitution of 7–12 moles of FITC per mole of albumin.

The protein was immobilized on the ZnO-based films by spontaneous adsorption from 100 μg/mL solution in PBS (40-min incubation time), followed by gentle rinsing with PBS and drying by dewetting in controlled laboratory atmosphere. The fluorescence signal–enhancing capability of ZnO-based films was assessed *in situ* by using an experimental configuration consisting of the substrates in contact with the protein solution (50 μL drop) during an established incubation time (40 min), thus rinsing with PBS to remove unbound protein molecules.

2.3. Physicochemical characterization of the protein–ZnO biointerface

X-ray photoelectron spectroscopy (XPS) analyses were performed by using a PHI ESCA/SAM 5600 multitechnique spectrometer. Experiments were carried out with the standard Al Kα radiation source ($h\nu$ = 1486.6 eV) at a base pressure of 2×10^{-9} Torr. XPS spectra were collected at a photoelectron take-off angle of 45°, which, according to the effective attenuation length values, respectively, of 0.74 nm, for photoelectron from Zn 2p traveling in ZnO [30], and of 3.13 nm, for Si 2p photoelectrons in an organic layer [31], roughly corresponds to an actual sampling depth in the range from about 1.6 nm (bulk ZnO) up to about 6.4 nm (bulk SiO_2). Both survey and narrow region scans were recorded, namely Zn 2p, C 1s, Si 2p, O 1s and N 1s peaks, at pass energy and incremental step size of 150 eV/1 eV for survey and 11.85 eV/0.05 eV for the narrow scans, respectively.

The XPS signals were analyzed with a peak synthesis program based on a non-linear background and experimental bounds fitting by Gaussian components. The atomic elemental compositions were evaluated using sensitivity factors provided by the F V5.4A software. All binding energies were referenced to C 1s neutral carbon peak at 285 eV.

Morphologies of the ZnO films were investigated using a LEO Supra 55VP field emission scanning electron microscope (FEG-SEM).

2.4. Fluorescence microscopy–fluorescence recovery after photobleaching (FRAP)

Observations were carried out by using an Olympus FV1000 confocal laser scanning microscope (LSM) equipped with a diode Ar laser, oil immersion objective (60× O3 PLAPO) and spectral filtering system. Excitation wavelength was set at 488 nm, and emitted light was detected at 519 nm (micrographs) or in the spectral range 490–620 nm.

The detector gain was fixed at a constant value, and images were taken for all of the samples, at random locations throughout the area of protein adsorption as well as at the borderline between protein-exposed and bare surfaces, in order to compare quantitatively the fluorescence due to the antigen coverage and that to due background noise. The latter was analyzed to have control areas; therefore, the only difference between the control and target samples is the presence of protein.

The average fluorescence intensity was calculated by taking the mean pixel luminance intensity for all pixels within a 5-μm^2 area over at least 10 separate measurements. Intensity data were analyzed by one-way analysis of variance (ANOVA) with a Tukey–Kramer multiple comparisons test. For the fluorescence recovery after photobleaching (FRAP) investigations, the data were normalized to the initial (pre-photobleach) value, which enables the percentage of photobleaching and the percentage fluorescence recovery within the laser region to be determined. For each sample, the emission recorded from the bleached spots was compared with that coming from contiguous non-bleached areas. Bare glass substrates were used for comparison. The samples were bleached for 1 min using high intensity (95% power) on the laser, immediately after a micrograph was taken every 1 min up to 10 min. By translating the sample stage, an average of 15 spots per substrate were photobleached in a given experiment.

3. Results and discussion

3.1. Physicochemical characterization of ultrathin ZnO-based films

SEM analyses were used for monitoring the morphological differences between the surfaces resulting from deposition at the different MOCVD time/temperature conditions on the silicon substrates (Fig. 1).

Fig. 1a shows that ZnO-1 sample (i.e., the film deposited at 300 °C/40 min) is characterized by a granular structure with a bimodal ZnO grain size distribution, showing a predominance of small grains (about 15 nm of average dimension) and few large grains (about 50 nm of average diameter) randomly distributed over the surface. As to the ZnO-2 sample (i.e., 400 °C/5 min), a smoother morphology is well evident (Fig. 1b) with about 50-nm-large grains clearly visible on the substrate. Finally, the ZnO-3 sample (i.e., 400 °C/60 min, Fig. 1c), used as control thick film, shows a homogeneous granular morphology characterized by fairly well-defined round grains having average dimensions of about 10–15 nm [30]. The morphological results provide confidence about two different ZnO deposition mechanisms, depending on the specific deposition temperature used. In particular, for the films deposited at the low temperature (300 °C), the ad atoms' mobility at the substrate surface during the MOCVD process is likely to be rather limited, thus resulting in a prevalence of an island-like ZnO layer formation (3D growth mode). On the other hand, upon increasing the deposition temperature (400 °C), the formation of a continuous

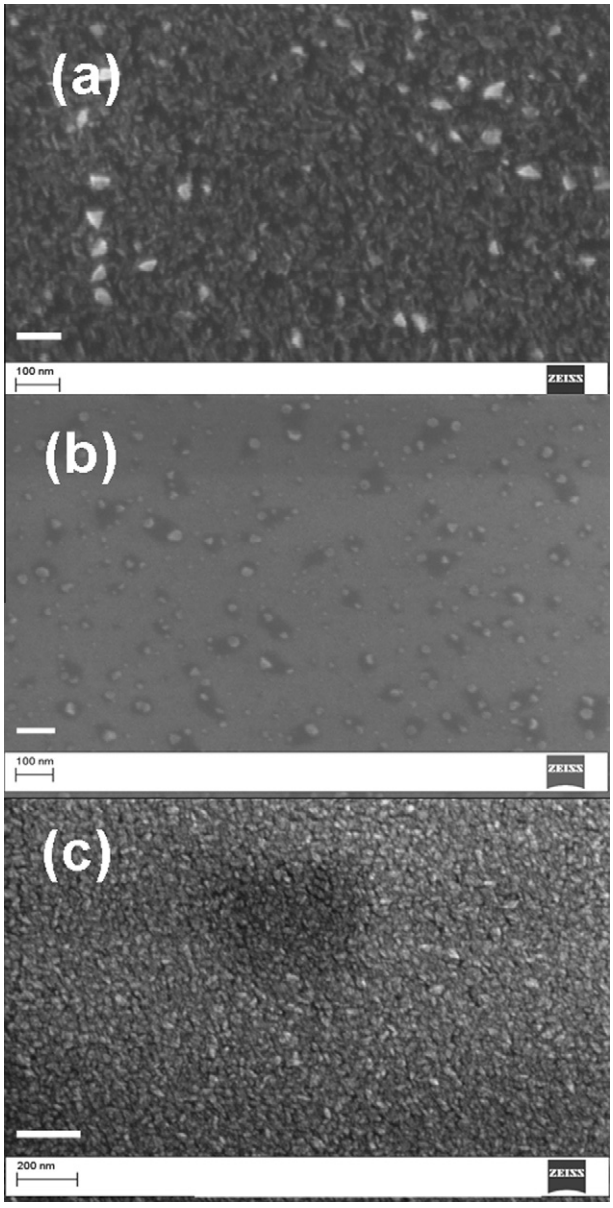

Fig. 1. SEM images of the ZnO-based films: (a) ZnO-1, (b) ZnO-2, (c) ZnO-3.

layer is favoured, both kinetically and thermodynamically, due to coalescence of the isolated ZnO grains (growth mode transition from 3D to 2D) and the final ZnO surface morphology becomes smoother.

The surface chemical composition of the whole-set ZnO samples as well as the control silicon substrate is given in Table 1.

Table 1
XPS quantitative analysis in terms of average atomic composition (at.%) and characteristic ratios for the ZnO films.[a]

Sample	Si	O	C	Zn	Zn/Si	C/Zn
Si	53	14	33	–	–	–
ZnO-1	0.1	51	35	14	140.0	2.5
ZnO-2	11	44	25	20	1.8	1.3
ZnO-3	0.1	45	26	29	290.0	0.9

[a] The relative standard deviation (RDS) calculated over three separate analyses of different samples results lower or comparable to the experimental XPS error, i.e., ±2%).

It is interesting to note that the detected silicon signal, characteristic of the substrate, is negligible (below the significance of the experimental error at the used conditions, i.e., 2% of atomic composition) for both ZnO-1 and ZnO-3 samples, but not for the ZnO-2, where a silicon signal attenuation of about 80% compared to the bare substrate is measured. This finding indicates that the complete coverage of the underlying silicon, in terms of the present XPS sampling depth (see Section 2.3), is obtained for ZnO-1 and the thick ZnO-3 samples. As a consequence of the mild ZnO-1 deposition conditions, a relatively low zinc content and a corresponding high C/Zn ratio point to significant carbonaceous residuals at the surface, which are mostly due to unreacted precursor as well as unavoidable surface hydrocarbon contamination.

In the case of ZnO-2 sample, notwithstanding the significant silicon signal detected, both the C/Zn atomic ratio and the zinc atomic content point to a surface chemical composition comparable to that of ZnO-3 sample (i.e., temperature-driven efficiency to control the precursor decomposition), but with a lower film thickness and uniformity (i.e., insufficient deposition time to attain the complete coverage).

To summarize, XPS analysis evidences that the newly prepared ZnO-1 and ZnO-2 films consist of heterogeneous ultrathin (less than 10 nm) ZnO-based films having different chemical compositions with respect to the presence of carbon-related species, as well as different surface coverage.

3.2. Protein interaction with the ultrathin ZnO-based films

Based on previously described studies, albumin is expected to irreversibly bind on ZnO surfaces by spontaneous adsorption driven by electrostatic interactions, at the physiological pH of 7.4 [21].

Aim of this work is to investigate the interface between such films and albumin, used as model analyte biomolecule, in terms of (i) the change in emission properties of ZnO; (ii) the biomolecule lateral mobility in the adlayer; and (iii) the protein surface coverage and its average orientation. XPS and confocal microscopy with the application of the FRAP technique were used to this purpose.

The XPS quantitative analysis of the samples exposed to FITC-albumin solution (Table 2) indicates that, after the spontaneous protein adsorption followed by rinsing out of the weakly bound molecules, a certain amount of irreversibly immobilized protein is detected at the surfaces of all the ultrathin ZnO-based films as well as the two reference controls, namely bare silicon (i.e., about 10-nm-thick native silicon oxide on silicon) and ZnO-3 (about 50-nm-thick ZnO).

The comparison between the protein-characteristic nitrogen signals detected at the surfaces of all the above-mentioned samples (about 5–6%) and the value of about 14% found for an ideally thick FITC-albumin adlayer (at least for the sampled depth of about 1.4 nm at the used experimental conditions) indicates a protein coverage roughly corresponding to the half of a monolayer [21]. However, it should be noted that the analytical quantification of protein coverage on the investigated substrates is affected by the

Table 2
XPS quantitative analysis in terms of average atomic composition (at.%) for the different ZnO films after albumin absorption.[a]

Sample	Si	O	C	Zn	N
Si + FITC-albumin	14	37	41	–	6
ZnO-1 + FITC-albumin	6	29	58	2	5
ZnO-2 + FITC-albumin	10	40	37	7	6
ZnO-3 + FITC-albumin	–	48	38	8	6
FITC-albumin	–	58	28	–	14

[a] The relative standard deviation (RDS) calculated over three separate analyses of different samples results lower or comparable to the experimental XPS error, i.e., ±2%).

expected partial surface dissolution of ZnO, due to the large concentration of unsaturated bonds, —OH groups and polar moieties that can readily interact with the protein molecules, thus promoting a prompt biodegradability. In fact, the biodegradation of ZnO in aqueous media and biofluids is a well-known process with important implications for biomedical applications [9]. ZnO is poorly soluble in water, but it can slowly dissolve in both acidic and strong basic conditions [32]. However, presence of biological components such as proteins and amino acids can also enhance the oxide dissolution through the complexation of the Zn^{2+} free ions released from the material surface [33–35].

Accordingly, we detect a silicon content of about 6% at the ZnO-1 surface after the protein adsorption (Table 2), while no significant silicon signal had been detected for the bare ZnO-1 film (Table 1). On the contrary, the silicon content detected at ZnO-2 surfaces does not change after exposure to the protein solution and similarly, no silicon is detected onto the albumin-immobilized ZnO-3 samples. These findings can be explained by considering the different surface termination and composition of the low-temperature deposited films (i.e., ZnO-1) compared with those deposited at the higher temperature (i.e., ZnO-2 and ZnO-3). In particular, the observed biodegradation of the ZnO-1 surfaces is likely the result of stronger protein–surface interaction at the biointerface than that in the case of ZnO-2 and ZnO-3 samples.

The detailed analysis of carbon and oxygen photoelectron peaks before and after the interaction with the protein further supports these data interpretation and adds significant hints about the average protein orientation at the ZnO surfaces.

The XPS peak details of C 1s regions are reported in Fig. 2.

As to the bare samples (Fig. 2a′–d′), the C 1s peak is a convolution of three main different components, corresponding respectively to: (i) C—C and C—H bonds (C_1 component, centered at binding energy, BE, of 285.0 eV), (ii) C—O bonds (C_2 component, centered at BE = 286.5 ± 0.2 eV) and (iii) carbon doubly bonded to oxygen species such as C(=O)O or O—C—O bonds (C_3 component, centered at BE = 288.8 ± 0.2 eV) [36].

It interesting to note that the ZnO-1 surfaces exhibit a higher content of polar linkages than the ZnO-2 and ZnO-3 ones, as evidenced by the relative ratio of carbon–heteroatom bonds (i.e., $C_2 + C_3$ components) with respect to the hydrocarbon species (C_1 component). This predominance is likely responsible for the biodegradability of ZnO-1 samples, i.e., the above-mentioned high reactivity towards surface dissolution processes prompted by the interaction with the protein.

After the protein immobilization, a broadening of C 1s peak is observed for all the investigated samples (Fig. 2a–d); this effect has been taken into account by adding a new component in the peak fitting, i.e., the peptide bond (—C(=O)—NH)-related peak (C_4, centered at BE of 288.3 ± 0.2 eV).

Moreover, the comparison of spectra shows that the C_2/C_4 ratio is about 2 for ZnO-1, ZnO-2 and reference Si surfaces, while it is reduced to 1 for control ZnO-3. This fact indicates that, notwithstanding the comparable protein mass uptake, the average orientation of C—O, C—N, C—S bonds (C_2) with respect to C=O species (C_4) of the protein adlayers is different at the interface with the thin ZnO–SiO_2 and Si substrates with respect to the thick ZnO-3 control film. This evidence suggests that SiO_2-uncovered areas in both ZnO-1 and ZnO-2 thin films (see XPS discussion above) contribute significantly to the actual surface termination, thus consisting in hybrid ZnO–SiO_2 biointerface.

The evidence of hybrid ZnO–SiO_2 active surfaces for the newly deposited ZnO ultrathin layer is further supported by the O 1s high-resolution spectra (not shown, see Fig. S1 in Supplementary material). Indeed, for the as-deposited ZnO films, the O 1s photoelectron peak can be consistently decomposed into two components, respectively, at 530.5 ± 0.2 eV (OM) and 532.0 ± 0.2 eV (OH). The lower-binding-energy component is attributed to O^{2-} ions of the crystalline network, which is identified as originating from O 1s core level of Zn—O [37], while the higher-binding-energy component is usually attributed to O^- species, i.e., the presence of loosely bound oxygen on the surface of ZnO film [38]. The surface-related component is prevailing in the ultrathin films ZnO-1 and ZnO-2 (OH/O_{tot}, respectively, of 66% and 63%), while it is slightly lower than the OM component in ZnO-3 film ($OH/O_{tot} \sim 45\%$). After the protein immobilization process, the OM component is hindered by the predominance of a new component centered at BE = 531.5 ± 0.2 eV, which is related to the protein C=O bonds.

This protein-related component is comparably higher than the OH one for both the ultrathin ZnO–SiO_2 films (about 3:1), while it is the only one visible for the control ZnO-3.

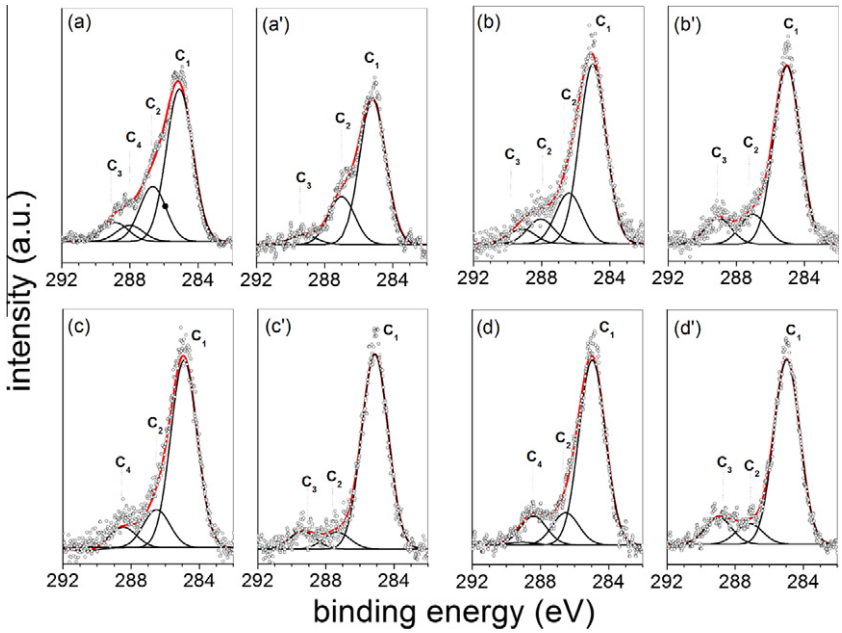

Fig. 2. XPS C 1s peak details for: (a) SiO_2, (b) ZnO-1, (c) ZnO-2 and (d) ZnO-3. Each panel contains both protein adlayers (left hand side) and bare (right hand side) samples.

To summarize, evidence of comparable protein mass uptakes onto the different ZnO-based films is provided by the attenuation of the substrate-related signals (Zn, Si and OM component of the oxygen peak) as well as the appearance of protein-related signals (nitrogen, C4 component of the carbon peak). The average protein orientation at the interface with the ultrathin ZnO-based films seems to be affected by the hybrid ZnO–SiO_2 character of the surfaces with respect to the control ZnO-3 sample.

Fluorescence microscopy was employed to scrutinize the response of the various ZnO deposited films to the binding of fluorescein-conjugated albumin as well as to implement data from XPS analysis about protein surface coverage, density and uniformity. Indeed, fluorescence analysis allowed determining in a semiquantitative way the protein uptake for the different ZnO films as well as the lateral mobility of the protein at the protein–zinc oxide interface.

Fig. 3 shows the representative LSM images recorded in fluorescence mode at the borderline between protein-exposed (brighter area) and masked (darker area) regions for control SiO_2 (Fig. 3a), ultrathin ZnO–SiO_2 film (ZnO-2, Fig. 3b) and thick ZnO control (ZnO-3, Fig. 3c) samples.

As our experimental scheme involves nonspecific adsorption of the protein molecules onto substrates, the protein molecules were randomly distributed over the entire protein-exposed surface area. Indeed, an enhanced fluorescence, related to the enhancement of emission recorded at 519 nm of wavelength, is observed for all the ZnO films as well as the control glass (SiO_2) upon the uptake of fluorescein-labeled protein. By assuming that the uniformity of the antigen coverage can be correlated with the standard deviation in pixel luminance for each of the samples, it appears that the protein coverage is less homogeneous on the ultrathin ZnO–SiO_2 films than on the thick ZnO sample.

What is more, the comparison of the fluorescence intensity for the differently protein-exposed films normalized vs. the corresponding control bare substrate and subtracted of the background emission (Fig. 3d) evidences roughly a twofold increase in average fluorescent intensity ($p < 0.001$) of the ZnO-based samples compared with SiO_2, notwithstanding the comparable amount of immobilized protein (as estimated by XPS). This fact points to the capability of our deposited ultrathin ZnO films to work as nanoplatform for fluorescence enhancement upon interaction with the protein.

The laterally homogeneous and ultrathin ZnO-based films have been compared with ZnO–SiO_2 nanoplatforms in order to scrutinize the lateral diffusion properties of protein adlayers on the patterned micropore arrays vs. the unpatterned ZnO films.

As matter of fact, the reduced critical dimensionality of ZnO materials at the nanoscale, either by topographic or by chemical structuring, such as ZnO nanorods or SAM-modified planar ZnO, is known to play a fundamental role in the fluorescence enhancement effect [1]. Therefore, the dimensional control of ZnO nanomaterials is very critical to trigger fluorescence detection from proteins. In this context, we have previously shown that ZnO nanoplatforms, consisting in thin films of hexagonally patterned ZnO nanoring arrays and SiO_2 circular areas, as obtained by colloidal template-assisted MOCVD process, are effective for immobilization of albumin [21]. As the effective process integration of colloidal lithography with MOCVD performed at extremely mild conditions has been demonstrated at the temperature/times of deposition as those used in the case of ZnO-2 samples [4,20], the ultrathin ZnO-2 films have been patterned into dense and regular micropore arrays (ZnO-2 NP samples).

The mobility properties of the protein molecules adsorbed on the two types of ZnO substrates have been assessed by FRAP experiments, which consist in using a focused laser beam at high power to intentionally photobleach quickly and locally fluorescently tagged proteins. Mobile proteins can exchange with their unbleached counterparts, leading to the recovery of fluorescence in the photobleached area at rates proportional to protein mobility.

FRAP is commonly employed to measure long-time two-dimensional diffusion of proteins adsorbed at solid–liquid interfaces, which depends on both protein–surface and protein–protein interactions [39,40].

Fig. 4 shows the results of the FRAP experiment performed on the protein adlayer onto both unpatterned (Fig. 4a) and patterned (Fig. 4b) ZnO-2 samples.

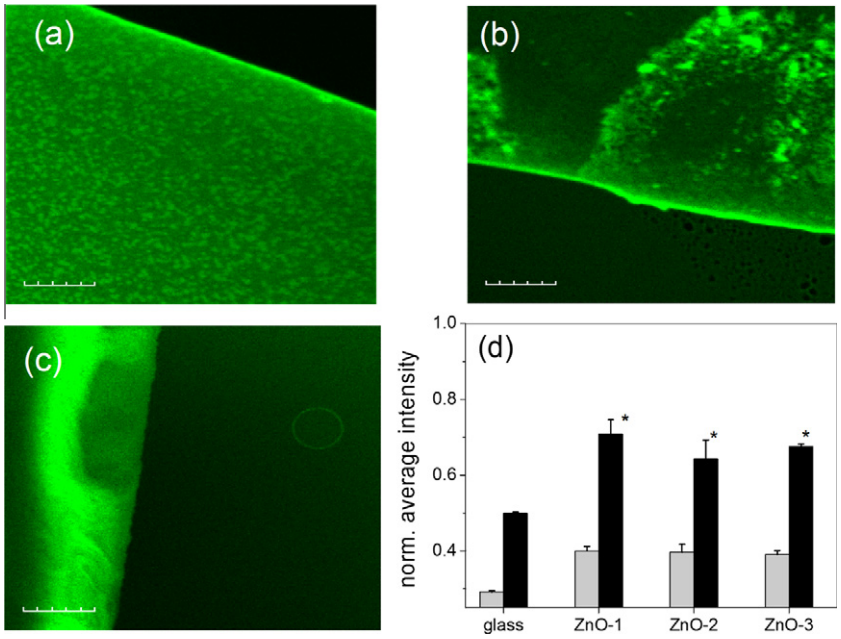

Fig. 3. LSM results for protein ZnO–SiO_2 biointerfaces. (a–c) Characteristic fluorescence at the borderline between masked and albumin-exposed regions for: (a) glass, (b) ZnO-2 and (c) ZnO-3. (d) Average emission intensity at 519 nm for each surface after protein immobilization (black columns) vs. incubation with buffer (gray columns). * = significant difference with respect to glass, as calculated with ANOVA, $p < 0.001$ (average of 15 photobleached spots per substrate in each experiments; error bars = standard deviation). (For interpretation of the references to colour in this figure legend, the reader is referred to the web version of this article.)

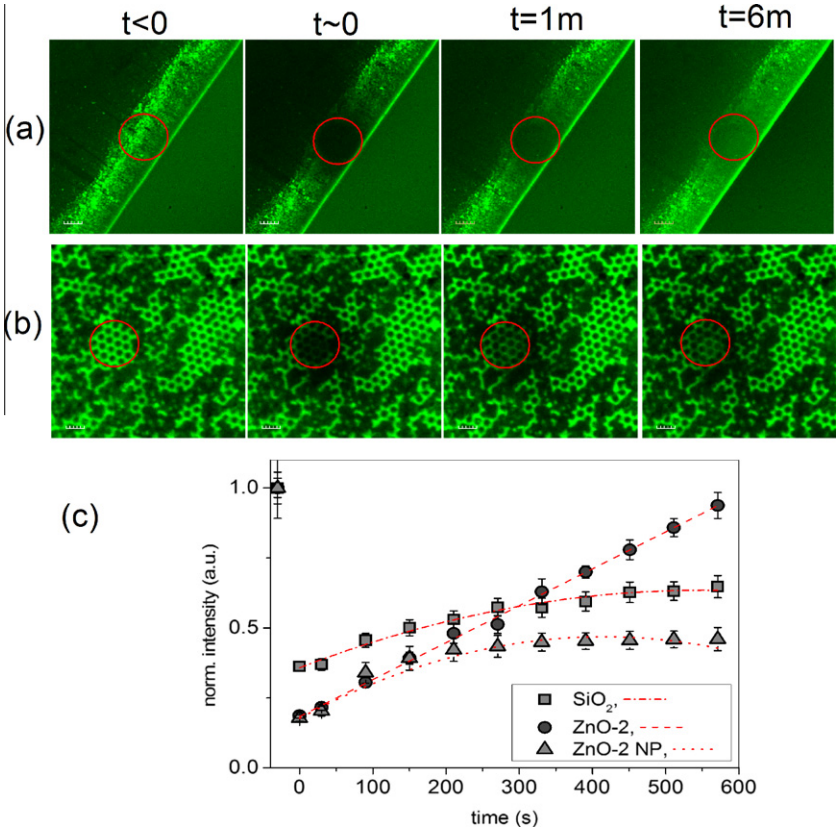

Fig. 4. Fluorescence recovery after photobleaching for albumin adsorbed on: (a) unpatterned ZnO-2 and (b) patterned ZnO-2 NP. Images are shown (from left to right) for pre-bleach, bleach, after 1 min and after 6 min of time lapse. (c) Time-solved fluorescence recovery from samples shown in (a and b) as well as control albumin-adsorbed on SiO_2 (glass). Average of 12 photobleached spots per substrate in each experiment.

It is worth of note that both types of protein–ZnO biointerfaces exhibit an extremely dynamic character, as well addressed by the micrographs taken at $t \sim 0$. In fact, the initial fluorescence before bleaching ($t < 0$) is expected to be quenched in a well-defined circular area by the high-intensity laser beam (circles drawn in Fig. 4a and b, $t < 0$). However, due to very fast random motion/diffusion of bleached protein molecules exchanging their position in the bleached area with non-bleached molecules from the surrounding, the bleached circles are not well defined already within the time required to record the first micrograph ($t \sim 0$). This finding suggests that the albumin aggregates on the ZnO substrates have a relatively fast diffusion at the surfaces and move around independently.

As to the fluorescence recovery ($t > 0$), two different kinetics are observed for the unpatterned and micropore-patterned ZnO-based films, corresponding to linear and polynomial fits, respectively (Fig. 4c). In particular, the protein molecules adsorbed on the ZnO-2 NP exhibit only a partial recovery and a lower effective diffusion than those adsorbed on the ZnO-2 surfaces. It is noteworthy that the fluorescence recovery from the protein adlayer on the reference glass substrate exhibits a polynomial curve trend similar to that observed for the hybrid ZnO–SiO_2 micropore sample. The diffusion coefficients calculated by using the Axelrod's algorithm [41] are, respectively, of 2.4×10^{-10} cm^2/s on glass, 1.5×10^{-10} cm^2/s on ZnO-2 and 1.0×10^{-11} cm^2/s on ZnO-2 NP. These findings indicate that, apart from the obvious enhanced friction suffered by the molecules moving inside the pore rims of the patterned ZnO-2 film in comparison with the unpatterned sample (i.e., topographic effect), the presence of SiO_2 areas confined by the ZnO is relevant to trigger the protein mobility at the biointerface (i.e., chemical effect). Similar results, pointing to a friction-reduced lateral diffusion on pore rims compared with that of the area within the pore, have been reported for lipid membranes on ordered porous silicon substrates [42]. In our case, the protein diffusion rate on the hybrid ZnO–SiO_2 surface is likely be affected not only by the topography by also by the surface chemistry and charge. In fact, the latter are crucial factors for the strength of interaction and the protein conformation at the protein–solid interface, thus affecting the transport process elucidated by FRAP [40,43,44].

It must be also mentioned that, since the ZnO isoelectric point is higher than that of SiO_2 (i.e., IEP ~9.5 vs. ~2 [45]), it is consistent that the fraction of immobile and laterally diffusing molecules at the solid–liquid interface is locally different on the hybrid ZnO–SiO_2 system.

FRAP experiments are currently underway to address more in detail the potential influence of 3D diffusion on the apparent 2D diffusion measured by FRAP in the protein adsorption process. Further studies with a wide range of new patterns, for instance by changing the density and/or the area of the ZnO–SiO_2 pore arrays, will allow the tuning of the surface reactivity towards transport processes at the biointerface to be used as models in biological studies or in applications such as biosensors.

4. Conclusions

This study is offered as an initial investigation for the preparation of ZnO-based sensors, by elucidating on an integrated MOCVD–CL deposition strategy to produce hybrid ZnO–SiO_2 platforms having tunable chemistry and topography, which in turn enable different fluorescence detections during biomolecule binding events. Experiments are currently underway to address this problem in more detail, in particular the determination of transport properties as function of the ZnO pattern, protein concentration, reversibility and reusability issues.

Acknowledgment

Authors would like to acknowledge INSTM for the support provided to the present research.

Appendix A. Supplementary material

Supplementary data associated with this article can be found, in the online version, at doi:10.1016/j.jcis.2011.09.014.

References

[1] A. Dorfman, N. Kumar, J.I. Hahm, Adv. Mater. 18 (2006) 2685.
[2] L. Wang, Y. Sun, J. Wang, J. Wang, A. Yu, H. Zhang, D. Song, J. Colloid Interface Sci. 351 (2010) 392.
[3] Z.L. Wang, Mater. Sci. Eng. R – Rep. 64 (2009) 33.
[4] M.E. Fragalà, C. Satriano, G. Malandrino, Chem. Commun. 7 (2009) 839.
[5] A. Dorfman, N. Kumar, J.I. Hahm, Langmuir 22 (2006) 4890.
[6] S.C. Lyu, Y. Zhang, C.J. Lee, H. Ruh, H.J. Lee, Chem. Mater. 15 (2003) 3294.
[7] X. Ren, D. Chen, X. Meng, F. Tang, X. Hou, D. Han, L. Zhang, J. Colloid Interface Sci. 334 (2009) 183.
[8] Z. Li, R. Yang, M. Yu, F. Bai, C. Li, Z.L. Wang, J. Phys. Chem. C 112 (2008) 20114.
[9] J. Zhou, N. Xu, Z.L. Wang, Adv. Mater. 18 (2006) 2432.
[10] B. Fang, C. Zhang, G. wang, M. Wang, Y. Ji, Sens. Actuators, B 155 (2011) 304.
[11] A. Umar, M.M. Rahman, A.A. Hajry, H.-B. Hahn, Talanta 78 (2009) 284.
[12] N. Kumar, A. Dorfman, J.-I. Hahm, Nanotechnology 17 (2006) 2875.
[13] F. Zhang, X. Wang, S. Ai, Z. Sun, Q. Wan, Z. Zhu, Y. Xian, L. Jin, K. Yamamoto, Anal. Chim. Acta 519 (2004) 155.
[14] V. Adalsteinsson, O. Parajuli, S. Kepics, A. Gupta, W.B. Reeves, J.-I. Hahm, Anal. Chem. 80 (2008) 6594.
[15] M.E. Fragalà, C. Satriano, J. Nanosci. Nanotechnol. 10 (2010) 5889.
[16] S. Krishnamoorthy, T. Bei, E. Zoumakis, G.P. Chrousos, A.A. Iliadis, Biosens. Bioelectron. 22 (2006) 707.
[17] V. Adalsteinsson, O. Parajuli, S. Kepics, A. Gupta, W.B. Reeves, J.-I. Hahm, Anal. Chem. 80 (2008) 6594.
[18] M.E. Fragala, Y. Aleeva, C. Satriano, J. Nanosci. Nanotechnol. 11 (2011), doi:10.1166/jnn.20115083.
[19] H.Y. Park, H.Y. Go, S. Kalme, R.S. Mane, S.-H. Han, M.-Y. Yoon, Anal. Chem. 81 (2009) 4280.
[20] M.E. Fragalà, C. Satriano, Y. Aleeva, G. Malandrino, Thin Solid Films 518 (2010) 4484.
[21] M.E. Fragalà, C. Satriano, J. Nananosci. Nanotechnol. 10 (2010) 5889.
[22] F.A. Denis, P. Hanarp, D.S. Sutherland, Y.F. Dufrene, Langmuir 20 (2004) 9335.
[23] A. Ruiz, A. Valsesia, F. Bretagnol, P. Colpo, F. Rossi, Nanotechnology 18 (2007) 505306.
[24] B.R. Pistillo, R. Gristina, E. Sardella, S. Lovascio, P. Favia, M. Nardulli, R. d'Agostino, Plasma Process. Polym. 6 (2009) S61.
[25] G.M.L. Messina, C. Satriano, G. Marletta, Chem. Commun. (2008) 5031.
[26] P. Hanarp, D.S. Sutherland, J. Gold, B. Kasemo, Nanostruct. Mater. 12 (1999) 429.
[27] G. Singh, V. Gohri, S. Pillai, A. Arpanaei, M. Foss, Peter Kingshott, ACS Nano 5 (2011) 3542.
[28] M.E. Fragalà, Y. Aleeva, G. Malandrino, Thin Solid Films 519 (2010) 7694.
[29] G. Malandrino, M. Blandino, M.E. Fragalà, M. Losurdo, G. Bruno, J. Phys. Chem. C 112 (2008) 9595.
[30] A.I. Martin-Conception, F. Yubero, J.P. Espinos, J. Garcia-Lopez, S. Tougaard, Surf. Interface Anal. 35 (2003) 984.
[31] G.M.L. Messina, C. Satriano, G. Marletta, Colloids Surf. B 70 (2009) 76.
[32] H.F.A. Trimbos, H.N. Stein, J. Colloid Interface Sci. 77 (1980) 386.
[33] I. Lynch, K.A. Dawson, Nanotoday 3 (2008) 40.
[34] T. Xia, M. Kovochich, M. Liong, L. Madler, B. Gilbert, H.B. Shi, J.I. Yeh, J.I. Zink, A.E. Nel, ACS Nano 2 (2008) 2121.
[35] A.E. Nel, L. Mädler, D. Velegol, T. Xia, E.M.V. Hoek, P. Somasundaran, F. Klaessig, V. Castranova, M. Thompson, Nat. Mater. 8 (2009) 543.
[36] K.G. Saw, K. Ibrahim, Y.T. Lim, M.K. Chai, Thin Solid Films 515 (2007) 2879.
[37] J.-C. Dupin, D. Gonbeau, P. Vinatier, A. Levasseur, Phys. Chem. Chem. Phys. 2 (2000) 1319.
[38] K. Kotsis, V. Staemmler, Phys. Chem. Chem. Phys. 8 (2006) 1490.
[39] R.D. Tilton, A.P. Gast, C.R. Robertson, Biophys. J. 68 (1990) 1321.
[40] E.P. Vieira, S. Rocha, M.C. Pereira, H. Möhwald, M.A.N. Coelho, Langmuir 25 (2009) 9879.
[41] D. Axelrod, D.E. Koppel, J. Schlessinger, E. Elson, W.W. Webb, Biophys. J. 16 (1976) 1055.
[42] D. Weiskopf, E.K. Schmitt, M.H. Klühr, S.K. Dertinger, C. Steinem, Langmuir 23 (2007) 9134.
[43] W. Norde, Macromol. Symp. 103 (1996) 5.
[44] C.K. Choi, J.D. Fowlkes, S.T. Retterer, P. Siuti, S. Iyer, M.J. Doktycz, ACS Nano 4 (2010) 3345.
[45] G.A. Parks, Chem. Rev. 65 (1965) 177.